Analysis and Study of a Bearingless AC Motor type Divided Winding, Based on a Conventional Squirrel Cage Induction Motor

Valcí F. Victor,
victor@ifto.edu.br
Instituto Federal do Totantins
Palmas-TO, Brasil

José Soares B. Lopes,
jose.soares@ifrn.edu.br
Instituto Federal do Rio Grande do Norte
Natal-RN, Brasil

Luciano dos S. Júnior
lucianojp@hotmail.com
Instituto Federal do Sertão Pernambucano
Floresta-PE, Brasil

João Coelho de S. Filho,
jcoelho@ifto.edu.br
Instituto Federal do Totantins
Palmas-TO, Brasil

Andres O. Salazar
andres@dca.ufrn.br
Universidade Federal do Rio Grande do Norte, Natal-RN, Brasil

Abstract

This paper shows the analysis and study of a bearingless AC Motor type divided winding for a conventional squirrel cage Induction Motor, IM. The conventional IM is used as a bearingless motor for artificial-lift oil proposes, allowing a reduction in maintenance and operation costs. The goal of this paper is improving electromagnetic forces performance, such as the Lorentz and Maxwell forces, allowing rotor positioning at the rotation axis. It was used a simulator based on the finite element method for acquiring load results for a 375 kW, 380V, 4-poles, 60Hz, 1.04 Nm, IM motor. Experimental results show that is possible to use a conventional IM as a bearingless motor, achieving a 80% efficiency. This paper presents simulated and experimental results that demonstrated the operation of the IM bearingless-type split coil built from a conventional induction motor.

1 Introduction

In some industry sectors, such as oil extraction industry, the common problems of maintenance, reliability, efficiency and longtime life issues in conventional electrical machines are leading to the use of bearingless motors. Bearingless motors were projected to solve the reducing volume issue of conventional IM [3]. In these motors, rotor positioning and torque generation are realized through magnetic forces provoked by stator current control of the motor [1], [2], [8]. So, in this sense, bearingless motors behave as a conventional IM motors. Stator bearingless motor presents two basic configurations: A first one, which consists of two separate stator windings: a torque generation winding and a rotor positioning winding [4]. Second one consists of only one single winding for torque generation and rotor positioning as well [5], [7], [9], [10].

The main characteristic of a bearingless AC motor, type divided winding is its similarity to conventional IM. This is mainly due to stator model, which utilizes the same windings for rotor speed and rotor positioning control. Thus, building machine and control system costs are drastically reduced.

Bearingless motor is increasingly used in a number of applications. Mainly in applications where mechanical bears periodical-maintenance lead to a problem, e.g. for vacuum pumps operating at deep profundities and high temperatures and also, for artificial-lift oil pumps, where a free contamination flowing fluid is need [6]. In order to verify rotor magnetic field behavior, it was developed a simulation tool based on finite elements to simulate the proposed motor. Simulated 4 poles bearingless motor, type divided winding has the characteristics show in Table.1. Thus, present work make the analysis of electromagnetic forces in IM motor, such as Lorentz and Maxwell forces in order to allow rotor positioning at rotational axis [1], [4].

*Contact Author Information: victor@ifto.edu.br, IFTO, Brasil

In the Bearingless motor induction winding divided type rotor position is corrected by working with the magnetic force in the air gap, this in turn is produced by the current which feeds each of the stator coils. The differential method is used for varying the current in each coil pair diametrically opposed so that the force produced tends to move the shaft where the desired direction. The force produced by each of the coils is given by the variation of magnetic energy stored in the system is given by:

$$F_a = K I_a^2 \frac{1}{(g-x)^2} \quad (1)$$

where:

K – a constant that depends on the number of turns, the permeability of the medium and the effective area traversed by the flow;
I_a – the current that runs through the coil;
g – the length of the air gap;
x – the position of the shaft.

Identically a force F_a' is produced in the coil opposite varying the current I_a' so that the shaft can be repositioned in the center of the stator. In the case of a single-phase induction motor force in the direction of the axis of the coil in either direction can be obtained by properly varying the current in the case of motors that have a greater number of phases in the composition of the forces produced in the various groups contribute to generate the force necessary to position the rotor. Figure 1 shows the magnetic flux produced by the currents in differential pair of coils in the x direction for the induction motor 4 poles.

Exciting the winding N_4 with sinusoidal current distribution takes place ψ_4 symmetrical flow as shown by the red line in Figure 1. Increasing the current $\Delta I1$ group N_{4d} right as shown in Figure 1 (a), the flow produced ψ_{4d} increases the flux density in the region of the air gap to the right, while decreasing the current $\Delta I1$ group N_{4E} left, the flow ψ_4e produced reduces the flux density in the region of the air gap left. The symmetrical distribution of the flow 4-pole ψ_4 is unbalanced. The unbalance of the magnetic field results in radial force applied to the rotor in the positive x direction, Figure 1 (a).

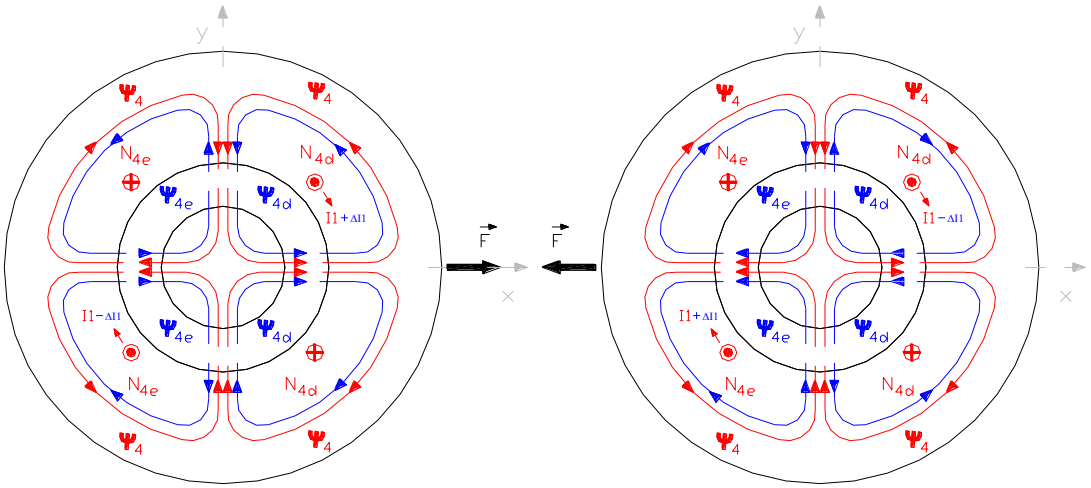

Figure 1: Bearingless motor induction winding divided type rotor:(a)Generation of radial force in the direction of the positive x axis, (b) Generation of radial force in the direction of the negative x axis.

Increasing the current $\Delta I1$ group left N_{4E} as shown in Figure 1 (b), the flow produced ψ4e increases the flux density in the region of the air gap to the left, while decreasing the current $\Delta I1$ group right N_{4d} , the flow produced ψ_{4d} decreases the flux density in the region of the air gap to the right. The symmetrical distribution of the flow 4-pole ψ_4 is unbalanced. The unbalance of the magnetic field results in radial force applied to the rotor in the negative direction of x, Figure 1 (b).

The generation of radial forces in the y direction is performed in the same manner as for the x-axis with the working group of the second phase whose axis is offset 90°. Thus the forces are generated to restore the rotor position from any position.

The four-pole winding N_4 has the dual function of producing electromagnetic torque and forces to restore the rotor position. The total power of the machine is divided to perform these two functions. The number of poles in the stator must be greater than or equal to four.

A model for the production of magnetic forces for positioning the rotor in the topic 2 is shown considering the variation of position of the shaft together with the variation of the currents of the stator coils. It is considered that the rotor is of a conventional squirrel-cage.

2 Motor modeling

A three phase, four poles, conventional squirrel cage IM, has its stator winding lodged in adjacent slots. The staggered coils are connected in series to form a phase group. Every phase group has two diametric opposite coils, as Figure 2 shows.

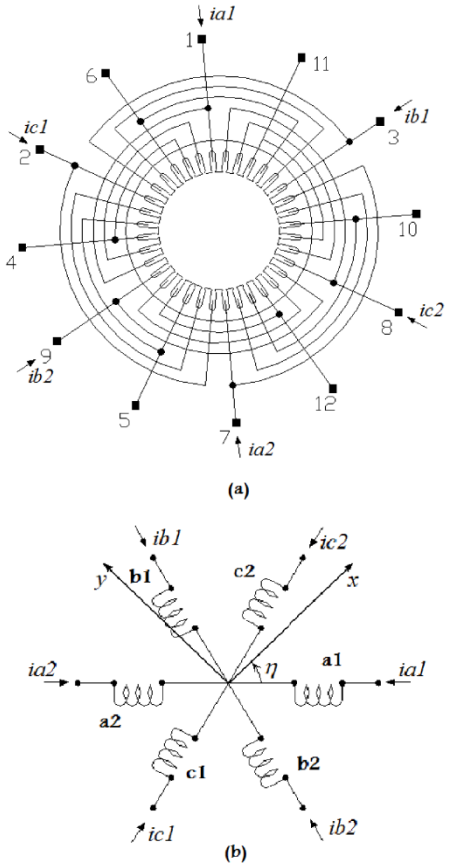

Figure 2: (a) Schematic distribution of stator coil and (b) circuit diagram.

Figure 2 (a) shows stator distribution winding, where there is a 120° shifting phase angle between each phase group axis. Figure 2 (b) shows winding current representation for each half a phase group. As it can be observed in Figure 2(b) a different current (namely i_{a1}-i_{a2}, i_{b1}-i_{b2}, i_{c1}-i_{c2}) is flowing in each half a phase group. However, as in a three phase system, each phase group current has a 120° shifting phase angle also. Thus, the first set of coils is a1– b1 – c1 and the second one is a2– b2 – c2. Figure 3 shows an equivalent circuit of a conventional three phase, IM motor (per phase). Where i_{a1} is stator current and i'_{a1} is the rotor current refer to stator. Others Motor parameters are listed in Table 1. It includes some laboratory measured test parameters as (per phase) equivalent inductances or resistances. For radial forces calculation of bearingless motor, it was considered: a) Iron magnetic permeability is

much greater than air permeability b) Ferromagnetic material is operating at linear zone (no saturation effect). c) Rotor position deviation is in *x* axis only. Then, rotor position deviation is related to *x* magnetic force by (2).

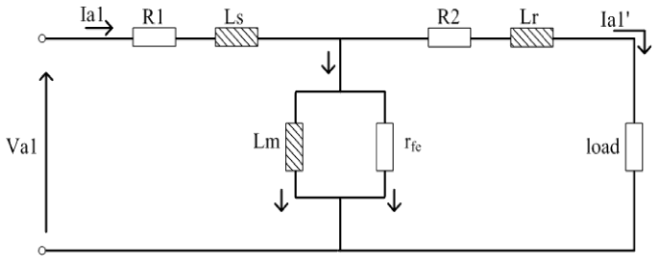

Figure 3: Equivalent circuit of the machine used.

Symbol	Parameter	Value*
R_1	Stator resistence	1,18 Ω
R_2	Rotor resistance	1,42 Ω
r_{fe}	Core loss resistance	891,2 Ω
L_s	Stator inductance	6,56 mH
L_r	Rotor inductance	6,56 mH
L_m	Magnetizating inductance	0,14 H
g_0	Air gap length	0,25 mm

*Ω = ohm, m = milli, H= Henry, mm = millimeter

Table 1: Equivalent Circuit parameters of the bearingless

$$F_x = \frac{K}{x_0^2}(I_{a1}^2 - I_{a2}^2) + \frac{2K}{x_0^3}(I_{a1}^2 + I_{a2}^2)x + \frac{K}{x_0^2}(-I_{a1}^2 - I_{a2}^2) + F_{Ext} \tag{2}$$

Where the first term of (2) is the average radial force in *x* direction which is function of I_{a1} and I_{a2}, see Figure 2(b). The second and third term are functions of *x* position and differential current ΔI ($\Delta I = I_{a1} - I_{a2}$) respectively. They need to be controlled by pruning the radial position in *x* direction. In [3] it can find the model for position in both *x* and *y* axes due to three phase currents, see equations (3) and (4).

In these equations Δi_a, Δi_b and Δi_c are differential current in *a*, *b* and *c* inductances respectively, g_0 is air gap length, η is the phase angle between *a* phase and *x* axis; F_x and F_y are external forces on *x* and *y* axes respectively.

$$F_x = k\begin{bmatrix} 6\frac{I^3}{g_0^3}x + 4\Delta i_a \frac{I}{g_0^2}\cos(\eta) + \\ 2\Delta i_b \frac{I}{g_0^2}\left[\cos(\frac{2\pi}{3}+\eta) - \cos(-\frac{\pi}{3}+\eta)\right] \\ + 2\Delta i_c \frac{I}{g_0^2}\left[\cos(-\frac{2\pi}{3}+\eta) - \cos(\frac{\pi}{3}+\eta\right] \end{bmatrix} + F_{Ext} \tag{3}$$

$$F_y = k\begin{bmatrix} 6\frac{I^3}{g_0^3}y + 4\Delta i_a \frac{I}{g_0^2}\sin(\eta) + \\ 2\Delta i_b \frac{I}{g_0^2}\left[\sin(\frac{2\pi}{3}+\eta) - \sin(-\frac{\pi}{3}+\eta)\right] \\ + 2\Delta i_c \frac{I}{g_0^2}\left[\sin(-\frac{2\pi}{3}+\eta) - \sin(\frac{\pi}{3}+\eta\right] \end{bmatrix} + F_{Ext} \tag{4}$$

Rotor magnetic field analysis was realized by means of Maxwell tensor method [3]. Figure 4 shows magnetic forces vector composition for current deviation in each phase group. Magnetic field vectors can control magnetic force vectors. Former vectors are modified in order to achieve center rotor position. Figure 5 shows instantaneous magnetic forces F_x and F_y, as a function of differential currents, see equations (3) and (4).

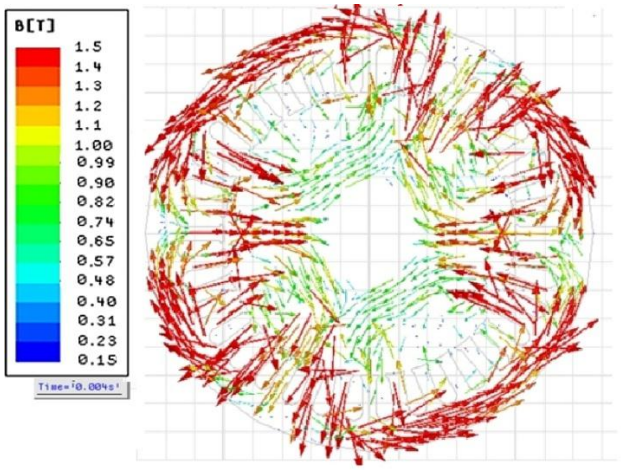

Figure 4: Behavior of vectors of force on the rotor with differential currents in a group of stator coils.

The simulation model was constructed from the motor plate data and manufacturer's data. Table 2 shows the most important data used to build the model.

Object	Dimension
External diameter of the stator	154,40 mm
Internal diameter of the stator	100 mm
Diameter of rotor	98,6 mm
Air Gag	0,20 mm
Length of rotor	130 mm
Area of the slot of the stator	72,30 mm^2
Area of the slot of the rotor	27,05 mm^2
Number of stator slots	36
Number of rotor slots	28
Number of turns per stator slots	103

Table 2: Specifications of the induction motor

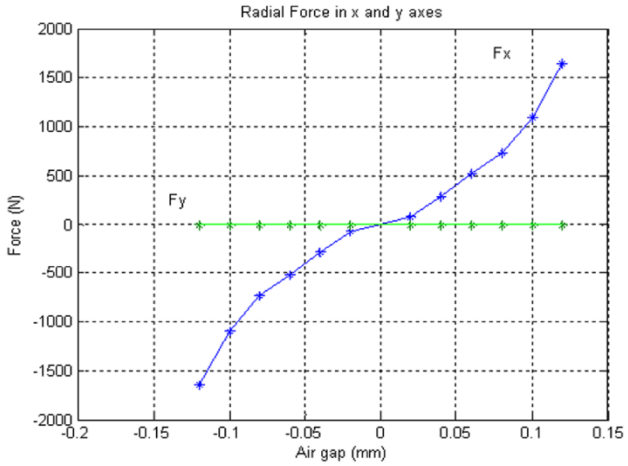

Figure 5: Radial forces in *x* and *y* directions with displacement of the rotor and coils with rated current.

Finite elements method was used in this simulation. Magnetic forces were evaluated with a 0,02mm resolution air gap, for a 4,06A current per phase winding group.

3 System configuration

Figure 6 shows a block diagram of proposed bearingless motor control system. Bearingless motor receives six command currents for Motor stator coils. These currents are driven using two parallel IGBTs (Insulated Gate Bipolar Transistors) inverters, as it is shown in Figure 6. The six independent current loops are implemented by a DSP (Digital Signal Processor) algorithm. The currents generated in the IGBTs are applied to the motor windings for producing torque forces and positioning the rotor.

Current references are given by the combination of torque and radial force commands [3]. Torque commands are generated by varying the reference angle in a balanced three-phase system, then creating the effect of a rotating magnetic field. Three phase current references are generated by a look up table.

The radial stabilization is based on two independent controllers acting on orthogonal axes sensing. The radial position sensors are based on magnetic induction of currents in high frequency and generate a linear response.

The algorithm of the PI-type current controllers and the PD-type position controllers is described by:

$$erro(k) = r(k) - y(k) \tag{5}$$

$$P(k) = K_p * erro(k) \tag{6}$$

$$I(k) = I(k-1) + K_i * erro(k) \tag{7}$$

$$D(k) = K_D * (erro(k) - erro(k-1)) \tag{8}$$

$$u(k) = P(k) + I(k) \tag{9}$$

$$u(k) = P(k) + D(k) \tag{10}$$

Where:
error (k) - control error;
P (k) - proportional action;
I (k) - integral action;
D (k) - derivative action;
u (k) - control signal

These controllers have a fixed structure, i.e., its parameters are static in time, are tuned to a point or region of operation. Both this work and with others before [11] presented such classics as the drivers were to achieve satisfactory control of current to the stator coils, and position control for centering the shaft.

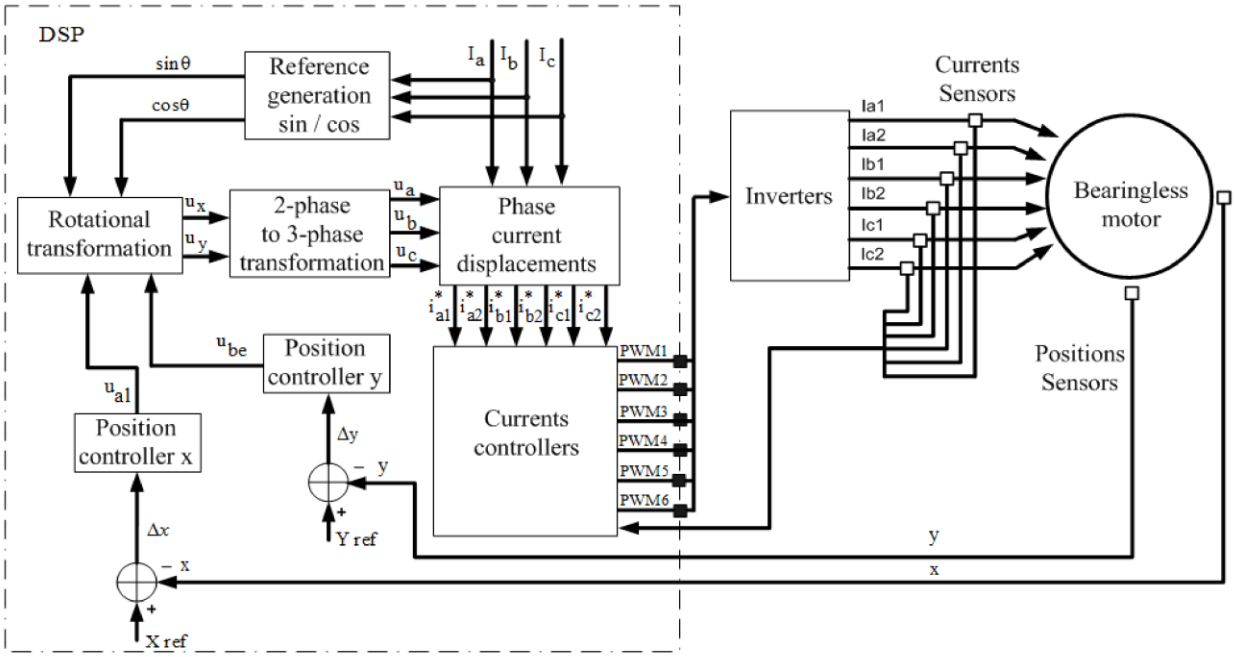

Figure 6: Control system used in bearingless machine.

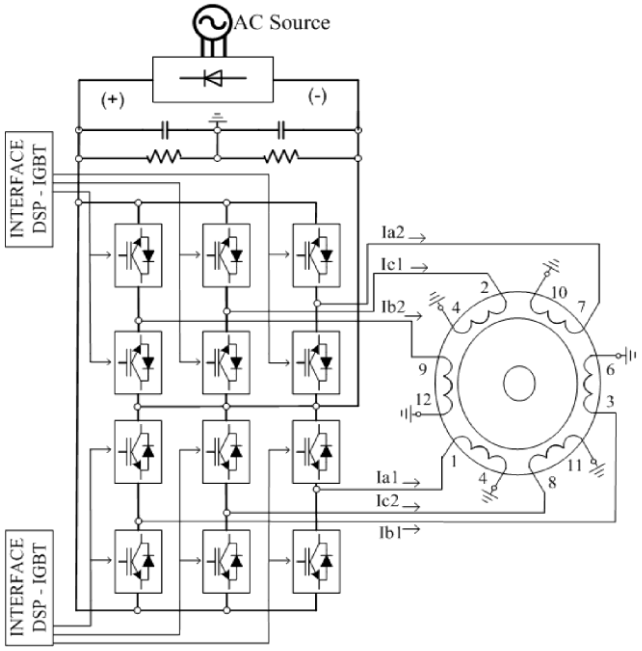

Figure 7: Power convert to drive the bearingless

4 Experimental results

The Figure 8 plots radial force versus one phase differential-current. It was obtained for both simulation and experimental results. Comparing both results, it can observe a 7% difference only when phase current is larger than 5A. Then, it is possible to verify properly the system functioning in a current range. Experimental results show that motor behavior within the recommended operation range, since it does not deviate from its theoretical behavior.

Then, proposed motor conversion allows low electromagnetic power losses and high reliability.

Positioning forces are obtained feeding the bearingless IM with unbalanced phase currents and the controlling rotor position. Figure 8 shows *a* and *b* half a phase group currents. It can be observe a 120^{o} phase difference among them, as it is expect to.

Figure 10 shows rotor sensor position of proposed bearingless motor system. External circle shows the maximum rotor orbit. Central point is real time rotor position controlled by proportional derivate (PD) controller, as it is shown in Figure 5.

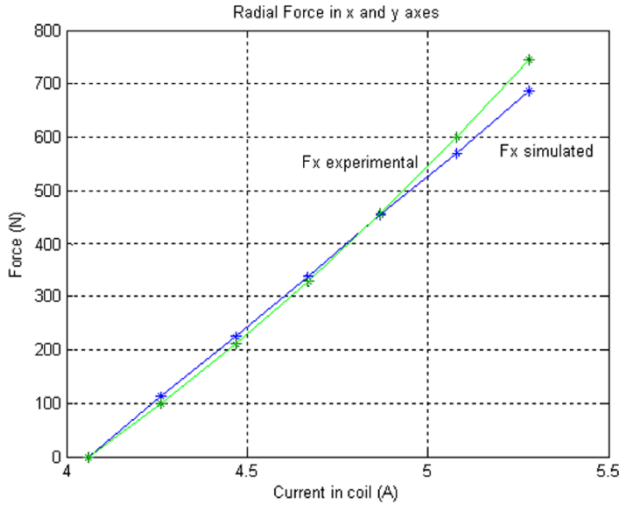

Figure 8: Simulated and measured radial forces in the x-rotor centered.

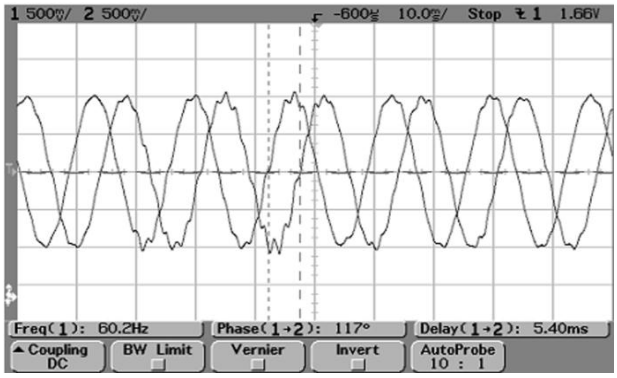

Figure 9: Controlled stator currents of two phases (0,5 V/Div).

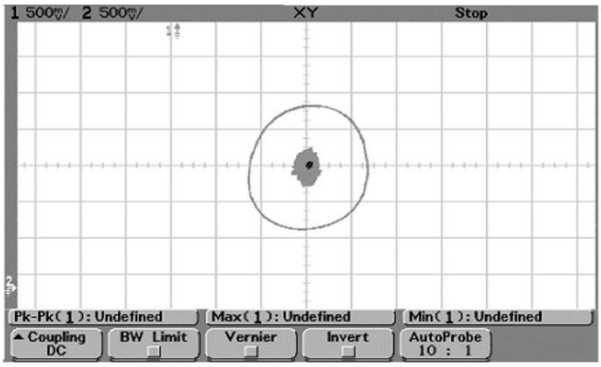

Figure 10: The rotor orbital around the central axis (0,1 mm/div).

Experimental results shows that proposed strategy makes it possible to obtain the rotor positioning at the shaft rotation axis control, without touching the lateral limits. Thus, it is eliminating the mechanical friction between rotating and fixed parts. Table II shows the main characteristics of designed machine. Nominal power, speed and voltage motor as well as power losses are also shown in Table 3. Accordingly, system efficiency ξ can be calculated as:

$$\xi = \frac{P_N - P_S - P_r - P_\omega - P_C - P_b}{P_N} \tag{5}$$

Thus, it presents 80% efficiency, similar to a conventional machine.

Parameter	Symbol	Value*
Nominal Power	P_N	3,7 kW
Nominal speed	ω_N	1720 rpm
Nominal Voltage	V_N	380 V
Nominal Current	I_N	8,11 A
Power Factor	PF	0,69
Inertia Moment	J	0,00995 kg.m^2
Spreading Factor	k	0.10
Pole Number	p	4
Stator Cupper Loss	Ps	234W
Rotor Cupper Loss	Pr	282W
Rotation Power Loss	Pω	46,92W
Core Power Loss	Pc	167W
Bearing Power	Pb	15,0W

* W = watts, k =kilo, rpm= rotations per minute, V = volt, A = ampere.

Table 3: Summary of main characteristics of the motors.

In figure 11 the structure of the experimental system is shown.

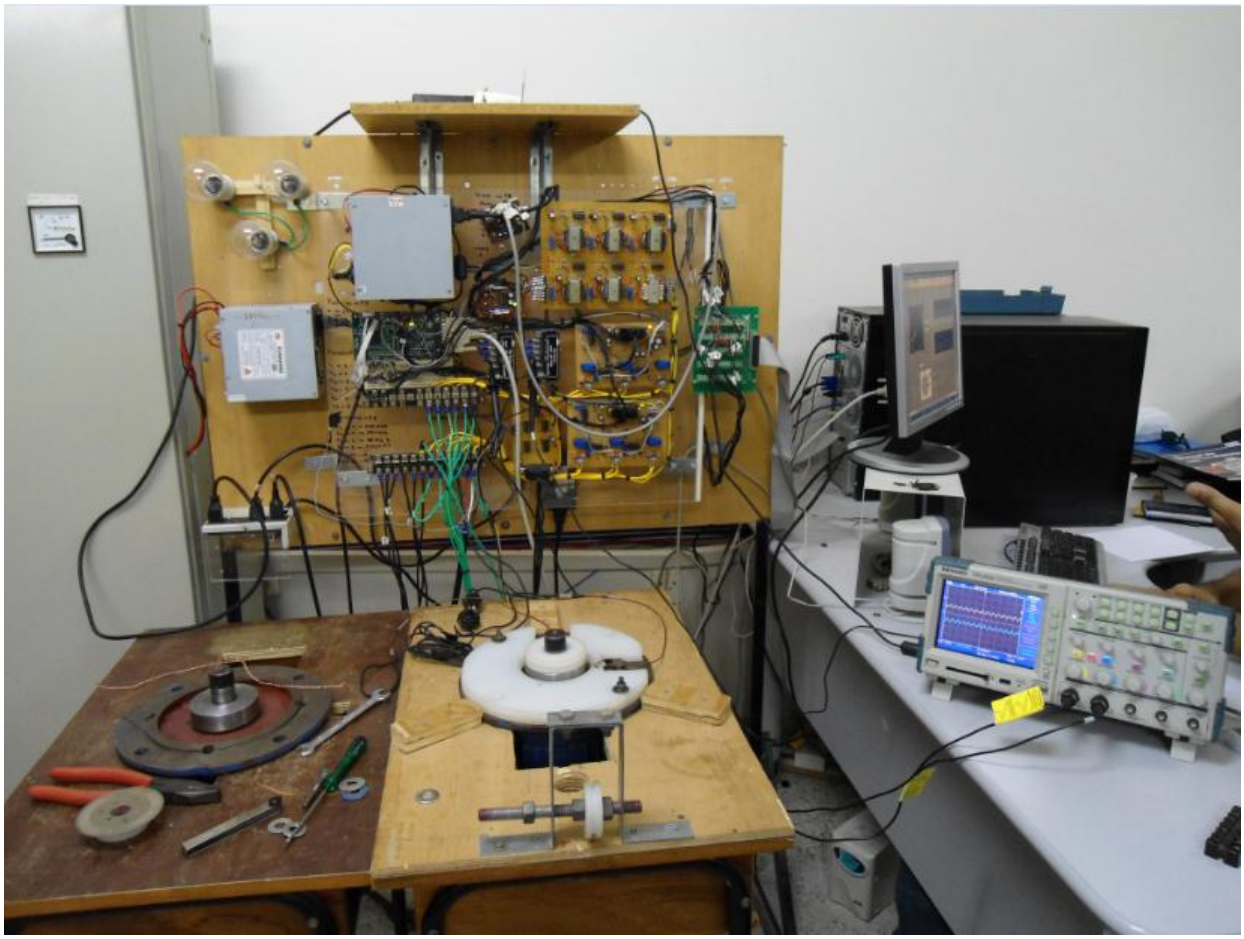

Figure 11: Overview of experimental system.

4 Conclusions

This paper presented the study and analysis of a induction motor squirrel-cage bearingless type showing satisfactory results. Experimental results show that the radial forces are sufficient to control the rotor position on the rotating magnetic field. Actually the prototype engine bearingless machine is being accelerated life tests for reliability assessment.

References

[1] A.O. Salazar, R.M. Stephan, - "A Bearingless method for induction machine", IEEE Trans.on Magn. Vol.29, N°6, pp.2965-2967, Nov. 1993.

[2] A. Chiba, T. Deido, and T. Fukao, - "Optimal Design of Rotor Circuits in Induction type Bearingless Motors", IEEE Transactions on Magnetics, Vol 34, No.4, pp. 2108-2110, Jul. 1998.

[3] Ferreira, J. M. S., Zucca, M., Salazar, A. O., Donadio, L. - "Analyses of Bearingless Machine with divide windings", IEEE Transactions on Magnetics, vol. 41, No. 10, pp. 3931-3933, Oct. 2005.

[4] Chiba A. , A.,Chida, K., Fukao, T., - “Principle and characteristics of a reluctance motor with windings of magnetic bearing”, IPEC, pp. 919-926, Japan, April, 1990.
[5] Chiba A., Power D. T., Rahman M. A., "Characteristics of a bearingless induction motor", IEEE Trans. on Magnetics, pp 5199-5201, Sep, 1991.
[6] Quintaes, F.; Salazar, A.O.; Maitelli, A.L.; Fontes, F.; Vieira, M.A.A.; Eslley, T.; "Magnetic Sensor Used to Detect Contamination of Insulating Oil in Motors Applied to Electrical Submersible Pump," *IEEE Trans. on* Magn., vol.47, no.10, pp.3756-3759, Oct. 2011.
[7] Oshima, M.; Miyazawa, S.; Deido, T.; Chiba, A.; Nakamura, F.; Fukao, T.; "Characteristics of a permanent magnet type bearingless motor," Industry Applications Society Annual Meeting, 1994., Conference Record of the IEEE , vol., no., pp.196-202 vol.1, 2-6 Oct 1994.
[8] A.O. Salazar, R.M. Stephan, W. Dunford, “An efficient bearingless induction machine”, COBEP, pp.419 - 424, Brazil, 1993.
[9] Amrhein, W.; Silber, S.; Nenninger, K.; "Levitation forces in bearingless permanent magnet motors," IEEE Trans on Mag. , vol.35, no.5, pp.4052-4054, Sep 1999.
[10] Ni Zhong-jin; Fang Liang; Chen Mao-jun; Xiu Shu-dong; , "Magnetic field analysis of bearingless permanent magnet motor," Consumer Electronics, Communications and Networks (CECNet), 2011 International Conference on , vol., no., pp.450-453, 16-18 April 2011.
[11] J. A. Paiva, V. F. Victor, A. O. Salazar, - “Neural estimation of flux applied to the vector speed control of a winding bearingless three-phase induction machine”, Revista de Eletrônica de Potência, vol 15, pp 107 – 114, 2010.